Improving the Tensile Mechanical Properties of Direct Energy Deposited (DED) Inconel 718 Aircraft Components Using a Standard Heat Treatment

A Senior Project
presented to
the Faculty of the Materials Engineering Department
California Polytechnic State University, San Luis Obispo

In Partial Fulfillment
of the Requirements for the Degree
Bachelor of Science

by
Spencer Vincent Flynn
June 2023

Acknowledgments

Many people made this project possible, and the following list is not exhaustive. First, thank you to Hermeus for sponsoring this project and allowing me to research a complex alloy with real-world applications. I want to thank Sam Stueland at Hermeus, who served as my primary contact, advised me on my project, and taught me a substantial amount about the topics I researched. Next, thank you to Professor Trevor Harding, who instructed me on properly conducting my senior project when I had no idea how to. Thank you to Professor Eric Beaton for maintaining the labs I worked in throughout the year. Finally, a big thank you to Professor Blair London, who served as my primary advisor and guided me through every step of this process. He helped me to grow and gain new skills, and I am confident that my experience with him will help me well beyond my senior project.

Abstract

This project aimed to improve the mechanical properties of as-printed additively manufactured Inconel 718 samples using a heat treatment usually used for cast and wrought Inconel 718. The mechanical properties sought to be optimized were yield strength, ultimate tensile strength, elongation, and reduction in area. The property goals were to match or exceed those of cast and heat treated Inconel 718. Wire-fed electron beam direct energy deposition (DED) was used to manufacture the samples, which were then heat treated using the AMS 5663 standard in an inert atmosphere. The samples were then tested in tension to obtain data on their mechanical properties. An as-printed sample was used as the control for the experiment before testing the heat-treated samples. The microstructures of the samples were then examined to determine the cause of any differences in the mechanical properties of the samples. The heat-treated samples displayed an increase in strength that matched the strength of cast Inconel 718. This increase in strength was caused by grain coarsening, dissolution of the Laves phase at layer interfaces, and precipitation of the δ phase and MC carbides in the gamma matrix (γ). The generalized heat treatment improved the mechanical properties of the DED Inconel 718, but the process could be improved. Future work should focus on tailoring the heat treatment for the specific manufacturing route and application of the material to optimize the mechanical properties even more. For example, high levels of the δ phase in the γ matrix signaled an overaging of the material that could have been prevented with a different heat treatment cycle.

Keywords

Superalloys, Inconel 718, Hypersonic Aircraft, Air Turboramjet Engines, Heat Treatment, Additive Manufacturing, Direct Energy Deposition (DED), Yield Strength, Ultimate Tensile Strength, Elongation, Materials Engineering

Table of Contents

List of Tables

List of Figures

1 Introduction

1.1 Hypersonic Aircraft

The first supersonic flight was accomplished in 1947 by the Bell X-1 when it reached 679 miles per hour or Mach 1.05 at 42,000 feet of elevation [1]. Since that historic flight, aircraft have been engineered to reach greater and greater speeds. Just 14 years later, a Soviet spacecraft became the first plane to reach hypersonic speeds (Mach 5) [1]. However, achieving these high speeds did not come without much innovation. The amount of propulsion necessary to achieve such speeds is tremendous and can only be achieved by an intricate design where multiple engine types interact [2]. Furthermore, this system must be highly efficient so the mass of the aircraft can be reduced to allow for greater speeds and to give the engineers greater freedom in their design of the aircraft [2]. This problem was overcome using rocket jets and ram jets in dynamic systems.

Hermeus is a new company based in Atlanta, Georgia, researching and developing a design for hypersonic passenger jets. Early prototypes for their air turboramjet engine utilized additively manufactured Inconel 718 components manufactured using a wire-laser direct energy deposition (DED) printer produced by Meltio. However, the mechanical properties of the samples they tested in-house were inadequate, and they have been attempting to find a heat treatment process that improves the mechanical properties of the alloy.

1.1.1 Rocket Jet Engines

Rocket jet engines utilize an oxidized rocket propellant to produce a jet that is directed through a nozzle at the back of the engine to generate thrust [3]. The schematic in Figure 1 shows the general design of these engines [4]. The most critical performance parameter of a propulsion system is the specific impulse it provides. Specific impulse is a general measure of the amount of thrust an engine can produce, and for a rocket jet engine, the specific impulse is in the range of 200-400 lb-sec/sec [3]. These engines are widely used because they are relatively simple and lightweight [5]. However, their low efficiency and inability to use oxygen from the air around

them to oxidize the liquid propellant severely limit their use [5]. These problems restrict the design of the aircraft because approximately 90% of the vehicle's mass is reserved for the propellant and oxidizer [6].

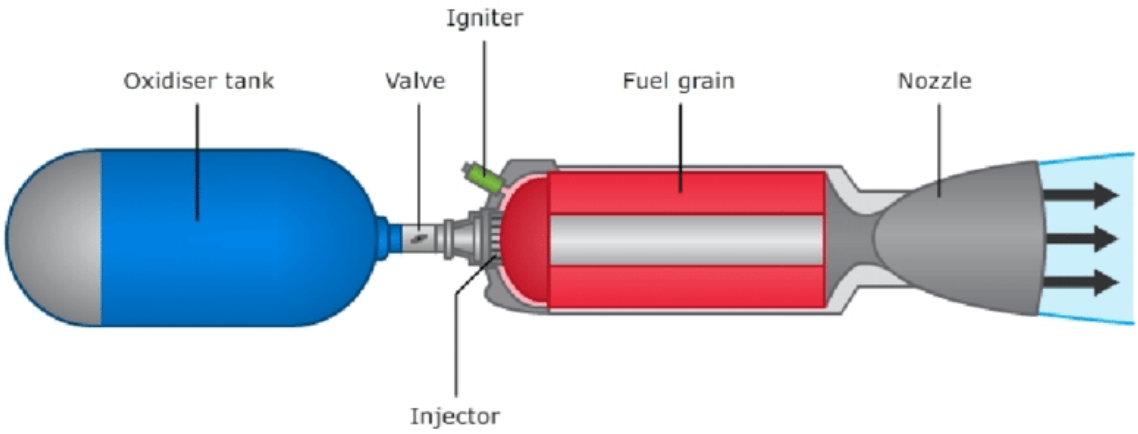

Figure 1: A typical design of a rocket jet engine [4].

1.1.2 Ramjet Engines

A ramjet engine is, in many ways, superior to rocket jet engines. One significant advantage is that it can use oxygen in the atmosphere to oxidize the propellant, substantially reducing the engine's weight [7]. As previously stated, the propellant and oxidizer occupy approximately 90% of the mass of vehicles using a rocket jet engine, with the oxidizer accounting for approximately 75% of that mass [5]. Removal of this excess weight makes the design of the aircraft much more manageable. Additionally, ramjets do not have moving parts, making them simpler to design and increasing their operating life [7]. Figure 2 shows a general design of a ramjet engine [8]. Finally, ramjets are more efficient than rocket jet engines, so their specific impulse is naturally higher at about 1,000-2,000 lb-sec/sec [6].

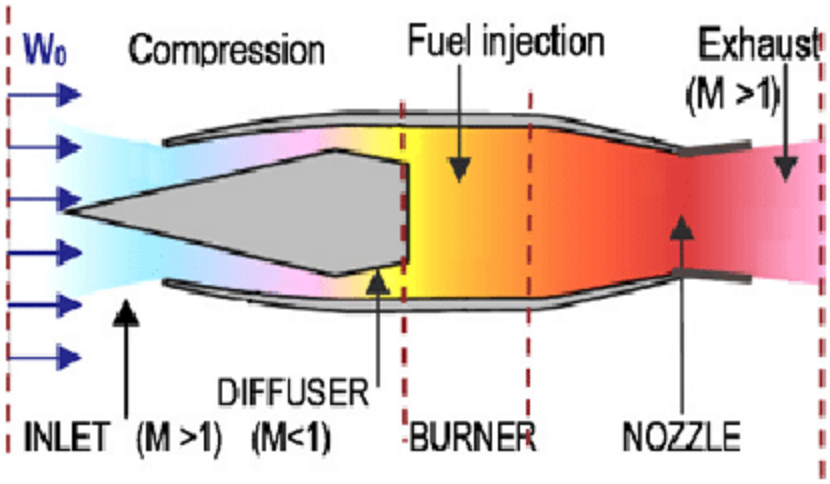

Figure 2: A typical design of a ramjet engine [8].

The biggest challenge facing these engines is their small operating window in terms of speed. Ramjet engines operate by collecting and compressing atmospheric oxygen into the engine and then using that oxygen to ignite the propellant. To accomplish this, the air must enter the engine at a velocity around Mach 2 at a minimum [7]. Additionally, the ramjet slows the flow of air as it enters the engine to approximately Mach 0.2, which induces large thermal and mechanical stresses on the engine and prevents it from operating at higher than Mach 5 [9].

1.1.3 Air Turboramjet Engines

To reach the hypersonic speeds that ramjet engines can achieve, a combined-cycle jet engine is required [6]. An air turboramjet is a common type of combine-cycle jet engine, and it utilizes a rocket jet engine in tandem with a ramjet to generate thrust. Figure 3 shows the basic design of an air turboramjet engine at both stages of operation. At the beginning of a flight, an aircraft equipped with an air turboramjet engine would operate as a standard jet engine. As the aircraft begins to gain altitude and speed, the temperature of the air entering the engine would reach the stagnation temperature of the rocket jet engine. The stagnation temperature is usually encountered when the aircraft reaches a sufficiently high velocity. The aircraft would then stop relying on the rocket jet engine for thrust and transition to only relying on the ramjet. This design takes the advantages of both the rocket jet and the ramjet engines while solving the limitations of both, making hypersonic flight feasible [10-12].

An added challenge of this design is the introduction of new moving parts due to the combination of two different engines. A smooth transition from operating as a rocket jet engine to a ramjet engine is necessary to prevent mechanical stress from building up in the engine and ensure that the aircraft's flight is not affected. Complex geometries of the inlet valves on the engine combined with pressure-sensitive flaps have solved this problem, but the added complexity is not ideal. The added complexity has revealed that many of the most common engineering alloys are insufficient for use in air turboramjet engines which has necessitated innovation in materials science [12-14]. The development of superalloys has allowed these complex systems to be implemented in aircraft for use in hypersonic flight.

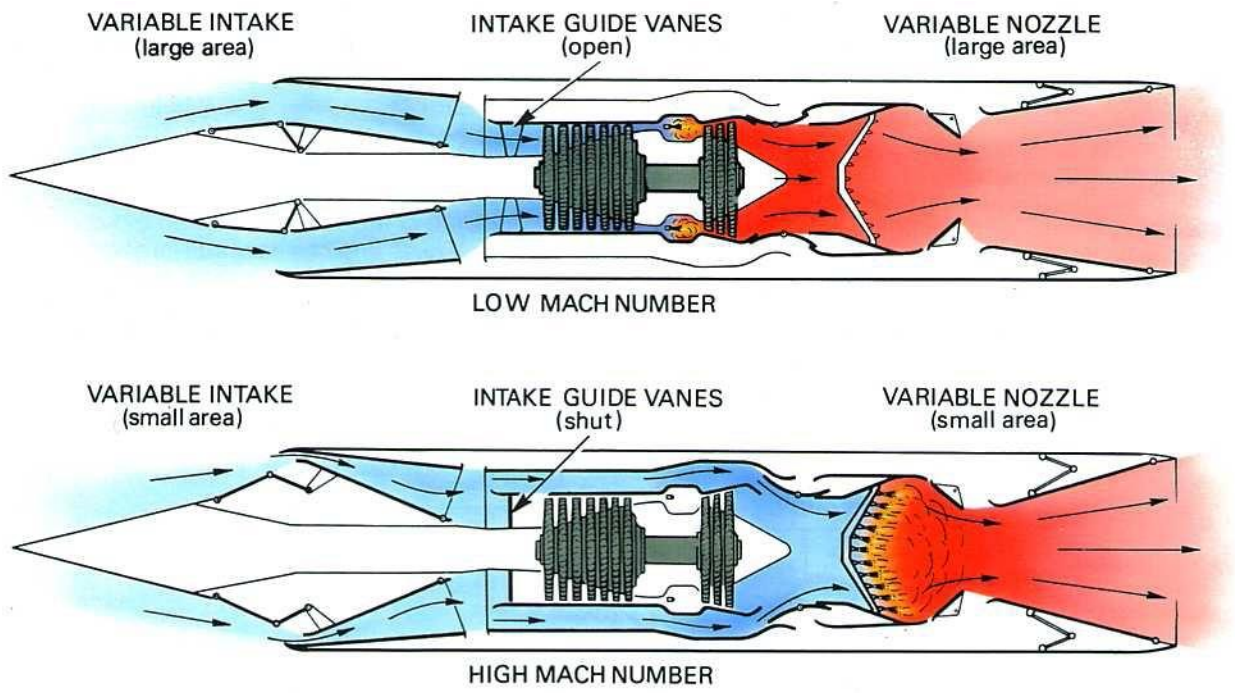

Figure 3: A typical design of an air turboramjet [11].

1.2 Superalloys

The engines described above are some of the most demanding engineering applications for materials[15]. The materials used in these engines must have high mechanical strength, be resistant to high-temperature oxidation, thermal and mechanical fatigue, hot corrosion, and creep [15]. Superalloys meet all these criteria and are widely used in the aerospace industry, nuclear reactors, submarines, and petrochemical equipment [15, 16].

Their development has been due, in large part, to innovations in both the processing and chemistry of these alloys [16]. Production of the first superalloys began in the 1940s for use in turbine blades and aerofoils [17]. New alloying and casting techniques in the 1950s improved the creep performance of these alloys by improving the quality and the cleanliness of manufactured parts [17]. Developments in directional solidification followed soon after that enabled metallurgists to make single crystals of these alloys, which improved their properties even more [17]. Current research is devoted to computer simulations to engineer new alloys and improving the additive manufacturing of these materials [15].

These alloys typically have a face-centered cubic crystal structure, and the precipitation of intermetallic, carbide, and gamma prime (γ') phases is crucial for their high strength and toughness [16]. Superalloys can be nickel-, cobalt-, or iron-based, but nickel-based superalloys are the most used in industry [15].

1.2.1 Cobalt- and Iron-based Superalloys

Cobalt-based superalloys are less utilized than iron- or cobalt-based superalloys, but they still serve an essential role in applications with high thermal and mechanical stresses. Cobalt-based superalloys are not strengthened by a coherent, ordered precipitate but by a solid solution-strengthened FCC matrix that has a small number of carbides distributed throughout [18]. Nickel helps stabilize the FCC structure while tungsten helps solution strengthen the alloy [19]. These superalloys have excellent resistance to sulfidation, a corrosive process that occurs in petrochemical applications [20]. This is due to the high chromium content (18-35 wt%), which forms a stable chromium oxide layer on the surface of the alloy that protects it from further corrosion [21]. Cobalt-based superalloys also have better mechanical strength than nickel and nickel-iron alloys at temperatures above 650°C because the γ'' phase in those alloys dissolves and is replaced by the delta phase, which is not as strong [20], [22]. In addition, they have better weldability and thermal-fatigue resistance than nickel-based superalloys [23]. Unlike nickel and iron-nickel alloys containing reactive metals like titanium and aluminum, cobalt alloys can be melted in the air rather than in a vacuum, making processing these alloys much easier [23]. The typical mechanical properties of wrought cobalt-based superalloys are detailed in Table I [18].

Table I: Selected Mechanical Properties of Cobalt-Based Superalloys

Property (units)	Value
Yield Strength @21°C (MPa)	317-2000
Yield Strength @540°C (MPa)	46-290
Ultimate Tensile Strength @21°C (MPa)	690-2025
Ultimate Tensile Strength @540°C (MPa)	740-1565
Elongation (%)	3.5-62

Iron-based superalloys evolved from austenitic stainless steels and are based on the concept of combining a close-packed FCC matrix with both precipitate-forming and solid solution-strengthening elements [23]. At least 25 wt% nickel is required in these alloys to stabilize the FCC matrix, and metals like titanium and aluminum are added for solid solution strengthening [23]. These alloys are difficult to manufacture and have lower operating temperatures than either nickel- or cobalt-based superalloys but are less expensive [23]–[25]. In addition, they are susceptible to oxidation, but this can be avoided by alloying the alloy with chromium [24]. However, these alloys have a low resistance to sulfidation, limiting their use and service life [24]. The typical mechanical properties of wrought iron-based superalloys are detailed in Table II [18].

Table II: Selected Mechanical Properties of Iron-Based Superalloys

Property (units)	Value
Yield Strength @21°C (MPa)	250-1110
Yield Strength @540°C (MPa)	180-960
Ultimate Tensile Strength @21°C (MPa)	595-1365
Ultimate Tensile Strength @540°C (MPa)	470-1205

1.2.2 Nickel-based Superalloys

The first nickel-based superalloy was called Nimonic, and it was developed in 1906 by A. L. Marsh. It was a nickel-chromium alloy with added titanium for solid solution strengthening that

was used in applications that required creep resistance, high strength, and stability at elevated temperatures [26]. However, this alloy was not commercially available until the 1940s as Nimonic 75 and Nimonic 80 [19].

Nickel-based superalloys have austenitic FCC microstructure with a dispersed intermetallic FCC that precipitates coherently with the matrix [19]. Carbides, borides, and other phases form at the grain boundaries of the alloy [19]. These alloys are more complex than other alloys due to the many phases and more than ten alloying elements, but their properties are so unique that the added complexity does not take away from their high demand [19].

Nickel-based superalloys are used for load-bearing applications at temperatures higher than 80% of their melting temperatures [23]. Much of these alloys' strength and stability at high temperatures is due to their high γ' content and the FCC structure that it forms in the alloy's matrix [19], [27]. Proper dispersion of the γ' phase is essential to significantly increase the strength of the alloy because of its particle-strengthening effect [27]. Added chromium in quantities greater than 15 wt% contributes to nickel-based superalloys' oxidation and sulfidation resistance while providing additional strength as a solid solution strengthener [26].

Some of the most essential applications of nickel-based superalloys are in nuclear reactors, dies for metalworking, pollution control equipment, and components for aircraft engines [26], [27]. Nickel-based superalloys now account for approximately half of the weight in advanced aircraft [23]. The typical mechanical properties of wrought nickel-based superalloys are detailed in Table III [18]. Nickel-based superalloys are by far the most used superalloys, and much research has been done on developing new and improved alloys for different applications [26]. Much of that research has focused on using these alloys in the aerospace industry for turbine blades, engine components, and fuselages [19].

Table III: Selected Mechanical Properties of Nickel-Based Superalloys

Property (units)	Value
Yield Strength @21°C (MPa)	285-1365
Yield Strength @540°C (MPa)	170-1255
Ultimate Tensile Strength @21°C (MPa)	660-1620
Ultimate Tensile Strength @540°C (MPa)	490-1550

1.2.2.1 René 41

The composition of René 41 is listed in Table IV [19]. It was developed by General Electric for use in turbofan engine blades, and it is commonly manufactured as a single crystal [27]. This alloy forms an M_6C carbide due to the added molybdenum, which replaces chromium in other carbides [23]. This configuration of carbides gives manufacturers greater control over grain size, allowing the alloy to be used in a broader range of applications [23]. It has average strength compared to other nickel-based superalloys but excellent strength retention at elevated temperatures [23]. However, this high strength comes at the expense of ductility, and it has a lower operating temperature than other alloys [23].

1.2.2.2 Waspaloy

The composition of Waspaloy is listed in Table IV [19]. This alloy has a lower strength but has some of the highest ductility and operating temperatures of nickel-based superalloys [23]. It also has the most extended operating life of any nickel-based superalloy [23]. Its primary use is in jet engines that experience high-temperature cyclic fatigue [26]. However, it is produced as a polycrystalline alloy, unlike most other superalloys used in such applications [27].

1.2.2.3 LC Astroloy

The composition of low carbon (LC) Astroloy is listed in Table IV [23]. It has high strength with moderate ductility, but these properties suffer at higher temperatures compared to other nickel-

based superalloys [23]. Its operating life is similar to Waspaloy's, which is ideal for high-fatigue applications [23]. The most significant benefit of LC Astroloy is its ability to be used as the material for additively manufactured components [23]. It achieves this through a higher concentration of titanium and aluminum, the primary γ'-forming elements [23]. This allows the alloy to have fine grains, which would hinder wrought and cast manufacturing but is beneficial in powder bed printing [23].

1.2.2.4 Inconel 718

Inconel was first discovered when ferrochrome (70 wt%Cr-30 wt% Fe) was added to nickel, giving the new alloy high strength and oxidation resistance at high temperatures [26]. Inconel 718 was developed when titanium and niobium were added to the alloy to solve the strain-age cracking problems during welding and weld repair of components [26]. The composition of Inconel 718 is listed in Table IV [19]. Inconel 718 is considered a nickel-iron alloy because of its high iron content, and the nickel-iron phase diagram in Figure 4 displays some critical phases discussed throughout this paper [26], [28].

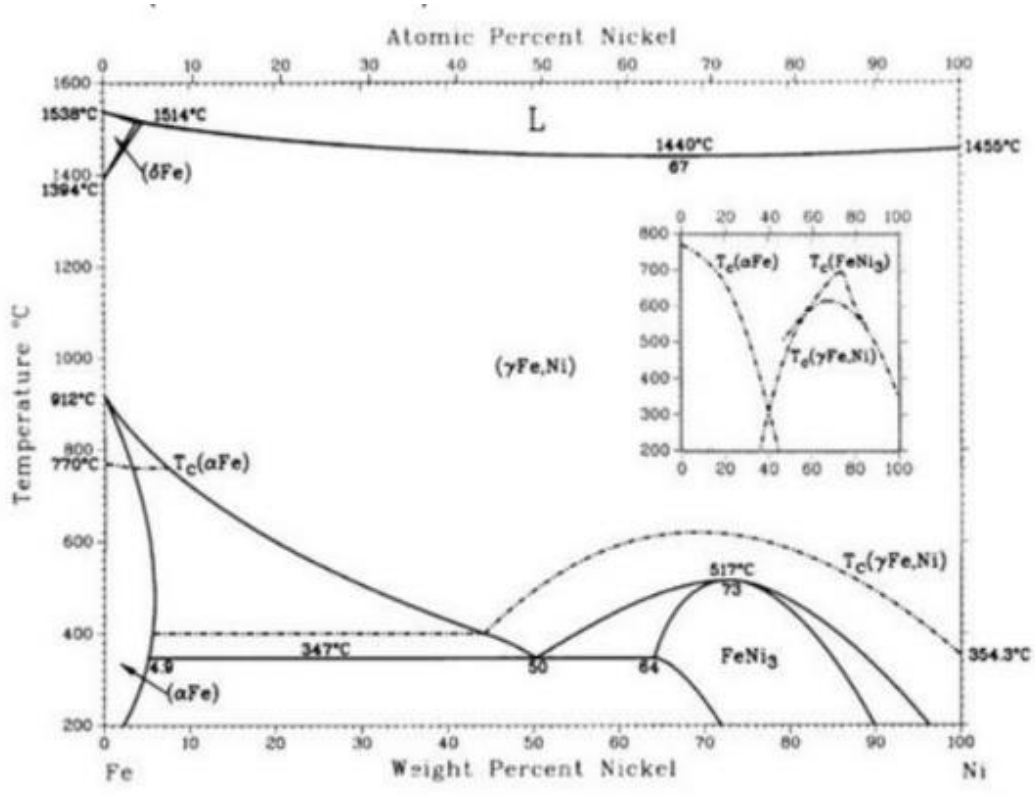

Figure 4: The iron-nickel phase diagram. The large gamma phase is the FCC matrix critical to the high strength and stability of Inconel 718 [28].

This alloy has high strength with good ductility and low cost, but it has a lower operating temperature than other nickel-based superalloys because it relies on the γ" phase for its strength [23], [27]. γ" forms along with γ' in alloys with niobium, but it is the primary strengthening phase in these scenarios [23]. As the temperature of Inconel 718 approaches 650°C, the unstable γ" phase dissolves, which degrades the strength of the alloy and makes it unsuitable for its original purpose [23]. It is commonly used in aerospace applications that require an extremely high-quality alloy to achieve the desired properties [19]. Its applications in industry include turbine blades, fuselage, and engine valves. The concentration of elements like oxygen, nitrogen, silicon, zirconium, and sulfur within the alloy is minimized to improve the mechanical properties and ease of processing of Inconel 718 [19]. Proper heat treatment of Inconel 718 is vital to achieving the desired material properties for high-performance applications [23].

Table IV: Chemical Composition of Selected Nickel-Based Superalloys

Alloy	Element Present (wt%)											
	C	**Cr**	**Co**	**Mo**	**Al**	**Ti**	**Zr**	**B**	**Mn**	**Nb**	**Fe**	**Ni**
René 41	.08	19	10.5	9.5	1.7	3.2	.01	.005	0	0	0	Balance
Waspaloy	.06	19	12.3	3.8	1.2	3	.01	.005	.45	0	0	Balance
LC Astroloy	.023	15.1	17	5.2	4	3.5	0	.024	0	0	0	Balance
Inconel 718	.04	18.5	0	3	.5	.9	0	0	0	5.1	18.5	Balance

1.3 Heat Treatment of Inconel 718

Heat treatment of Inconel 718 coincided with its early development because the technological advances in both occurred simultaneously [19], [26]. Improvements in casting and alloying techniques gave metallurgists greater control over the properties of the alloy [19]. Inconel 718 components are first treated at high temperatures (>1000°C) for 1-4 hours to dissolve nearly all the γ' and carbides in the alloy [23]. Then, the alloy is aged to strengthen it through coarsening of the grains, solid solution strengthening, precipitation hardening, or carbide precipitation [23], [26].

1.3.1 Solid Solution Strengthening

Solid solution strengthening is the least important factor in the heat treatment of Inconel 718 [19]. Molybdenum and chromium are the main promoters of solid solution strengthening, and these elements are distributed throughout the FCC γ matrix [19], [23]. Although molybdenum increases the strength of Inconel 718, its addition can have deleterious effects at incorrect concentrations, so it must be carefully controlled [19]. Excessive solid solution strengthening can lead to the formation of undesirable phases like alpha chromium and molybdenum-rich mu [19]. Additionally, the solid solution strengthening elements of Inconel 718 limit its forgeability in the cast and wrought conditions but make it easier for the alloy to be additively manufactured [23].

1.3.2 Carbide Precipitation

Precipitation of carbides is one of the primary strengthening mechanisms in Inconel 718 and confers improved rupture strength of the alloy at high temperatures [19], [23]. Nickel is not a carbide former, so the molybdenum, chromium, and niobium in this alloy serve as the primary formers of the desired carbide phase [23], [26]. Carbide precipitation is especially important in controlling the mechanical properties of Inconel 718 as the carbides diffuse along the grain boundaries and help form coarser grains [19]. The shape and distribution of carbides is a crucial part of the desired property attainment in Inconel 718, and particles of blocky $M_{23}C_6$ carbide in a discrete, discontinuous fashion are preferred as this configuration increases strength and resistance to fracture [19]. Figure 5 shows an SEM image of this preferred configuration [27]. This phase is formed through the rapid cooling of Inconel 718 components, and proper heat treatment at lower temperatures (760-980°C) must be applied to stabilize this carbide phase [19], [23]. These carbides can also be formed by the degradation of the less stable MC carbide phase or from residual carbon reacting with chromium and molybdenum to form $Cr_{21}Mo_2C_6$ [23]. When this carbide is formed from the degradation of the MC carbide, additional γ' is precipitated in the reaction

$$MC + \gamma \rightarrow M_{23}C_6 + \gamma' \quad (1)$$

which adds to the mechanical strength of the alloy by inhibiting grain boundary sliding [23]. Carbides can be a bane or a blessing, so care must be taken to control their concentration, distribution, and geometry [26]. For example, too high of a concentration of carbides in Inconel 718 can reduce the amount of chromium in the alloy's matrix, reducing its resistance to oxidation and corrosion [26].

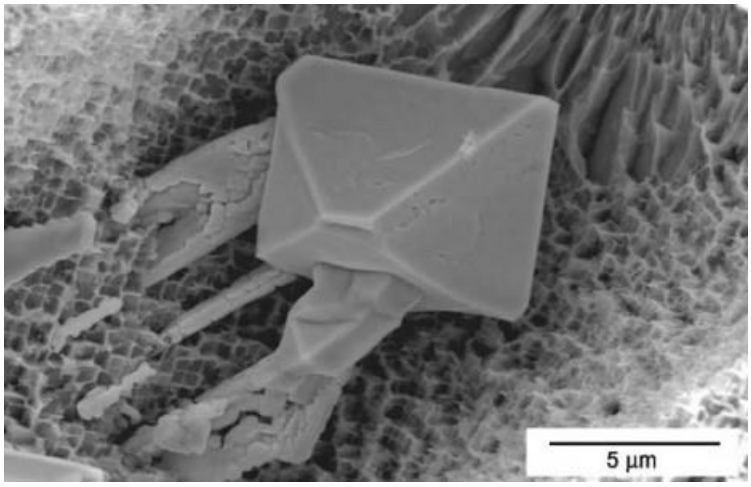

Figure 5: An example of a blocky MC carbide formed along the grain boundary of the gamma phase [17].

1.3.3 Precipitation Hardening

The precipitation of the γ' and γ'' phases in Inconel 718 sets it apart from other alloys [19]. γ' is an intermetallic with an FCC structure and a chemical formula of Ni_3(Al, Ti) [19], [23]. It disperses coherently within the γ matrix, and the two are almost indistinguishable in the microstructure [19]. The small lattice mismatch (<1%) between the γ matrix and the γ' precipitate allows for such a coherent configuration [26]. The amount and morphology of γ' within Inconel 718 are critical in achieving the desired properties [19]. Higher levels of γ' correlate with higher creep and rupture strength at high temperatures [19]. Finer γ' particles are preferred for higher rupture strength, which can be achieved through a slower cooling rate [19]. However, this slower cooling rate also leads to a greater property value dispersion due to random crystallographic orientations [19]. Rapid cooling during heat treatment maintains the fine γ' particles and improves Inconel 718's high-temperature strength [19]. This heat treatment also precipitates a film of γ' along the grain boundaries of the γ matrix and on the $M_{23}C_6$ particles, which increases the strength of the alloy even more by preventing grain sliding [23]. Chromium degrades the high-temperature strength of γ', which is why much of it has been replaced by iron in Inconel 718, but the added strength comes at the expense of corrosion resistance [23].

Because of the high iron content and presence of niobium in Inconel 718, the γ' phase is often replaced by γ'' [29]. γ'' is a body-centered tetragonal (BCT) phase that is coherent with the γ matrix with the chemical formula Ni_3Nb [19]. It forms disk shapes throughout Inconel 718 [23]. While γ' has a relatively small lattice mismatch with the γ matrix, γ'' has a lattice mismatch of

2.9%, which induces a considerable strain within the microstructure that improves the overall strength of the alloy [23]. γ" is a metastable phase, and it limits the applications of Inconel 718 because it dissolves to the more stable delta phase at temperatures greater than 650°C [23]. In addition, its slow diffusion makes Inconel more weldable and makes it easier to manufacture components through conventional processes and additive manufacturing without cracking [30].

The precipitation of phases in this alloy is not always favorable as the precipitation of the intermetallic delta, mu, and Laves phases can cause microstructural instabilities during the normal service life of Inconel 718 components [19]. These phases have platelike or needle-like morphologies, and they reduce the ductility and rupture strength of Inconel 718 [23]. These deleterious phases only form when the alloy has been overaged, or the beneficial phases previously discussed have been dissolved due to high temperature [19].

1.3.4 Standard Heat Treatments

Since metallurgists observed the phenomenon of solid solution strengthening, carbide precipitation, and precipitation strengthening in Inconel 718, much research has been devoted to developing standard heat treatments that can be used for this alloy [30]. The goal of these standards is to find the conditions that yield the optimal concentration, distribution, and morphology of precipitates and solid solution-strengthening elements [19], [23], [30]. Heat treatment of Inconel 718 begins with a high temperature normalizing to dissolve the precipitates formed during the production of the alloy [25], [30]. The alloy is then quenched to room temperature to achieve the proper carbide configuration before moving on to the next phase of the heat treatment [19], [25]. The alloy is then brought to a moderate temperature (750°C) to precipitate more carbides and to allow them to diffuse properly [19], [25], [30]. Finally, the alloy is brought to temperatures below 650°C to precipitate the γ" phase [19], [25], [30]. The temperatures and times for each step are slightly changed depending on the application of the alloy [30].

1.3.4.1 AMS 5663

This heat treatment was developed for aerospace applications for cast and wrought Inconel 718[25]. It provides the alloy with good rupture life, good notch rupture life, and rupture ductility with high yield, ultimate tensile, and fatigue strength [25], [30]. The schedule for this heat treatment is as follows: normalize at 1725-1850°F for 60 minutes followed by water quenching; age at 1325°F for 8 hours; furnace cool to 1150°F and hold for another 8 hours followed by air cooling [25], [30]. This treatment produces a fine grain structure which contributes to the high fatigue strength of the alloy [30]. Treating the alloy below the delta solvus temperature allows the delta phase to pin the grain boundaries, which causes the fine grain size mentioned above [30].

1.3.4.2 AMS 5664

This heat treatment was developed for cast and wrought Inconel 718 in tensile-limited applications [25]. It gives the alloy high ductility, impact strength, and tensile strength at low temperatures [25], [30]. The schedule for this heat treatment is as follows: normalize at 1900-1950°F for 60 minutes followed by water quenching; age at 1400°F for 10 hours; furnace cool to 1200°F and hold for another 8 hours followed by air cooling [25], [30] Unfortunately, this treatment produces a more brittle alloy because the normalizing temperature is above the δ solvus temperature [30].

1.3.4.3 MR 0175

This heat treatment is less commonly used and is utilized for applications in the petrochemical industry [30]. It produces an alloy with high hardness and improved corrosion resistance [30]. The schedule for this heat treatment is as follows: normalize at 1850-1900°F for 60 minutes followed by water quenching; age at 1450°F for 6-8 hours followed by air cooling [25], [30].

1.4 Additive Manufacturing of Inconel 718

Understanding Inconel 718 and its applications is important, but discussing the processing methods being used and developed to improve its overall performance is also important. As was previously discussed, the design of air turboramjets is exceptionally complex, and the components within the engine have geometries that are difficult to achieve using conventional casting and forging techniques. Therefore, engineers have begun to build Inconel 718 components using additive manufacturing techniques. Various techniques have been developed and implemented, but they all stem from powder metallurgy [31]. This type of processing requires the transfer of a digital file (CAD file) to a machine to build the three-dimensional component [31], [32]. Powder bed fusion (PBF) and direct energy deposition (DED) are the two most common techniques and will be discussed here. Both processes produce components with a fine grain structure which is beneficial for Inconel 718 and makes it an ideal manufacturing process for the alloy [33].

1.4.1 Powder Bed Fusion

Laser powder bed fusion (LPBF), electron beam melting (EBM), selective laser melting (SLM), laser rapid forming (LRF), and direct metal laser sintering (DMLS) are just a few important PBF techniques[33]–[37] However, the basic principle behind these techniques is the same: a component is built layer-by-layer on a print bed platform by melting metal powder using a laser. A basic schematic of the process is shown in Figure 6 [32]. The metal particles used in the powder typically have a diameter of 5-200 μm [32]. In a modified PBF technique, the particles may be coated in a polymer before processing [38]. Then, the polymer is melted instead of the metal, forming necks between the other particles and their polymer coatings [38]. Components made using this method are porous and require hot isostatic pressing (HIP) to achieve their full density [38].

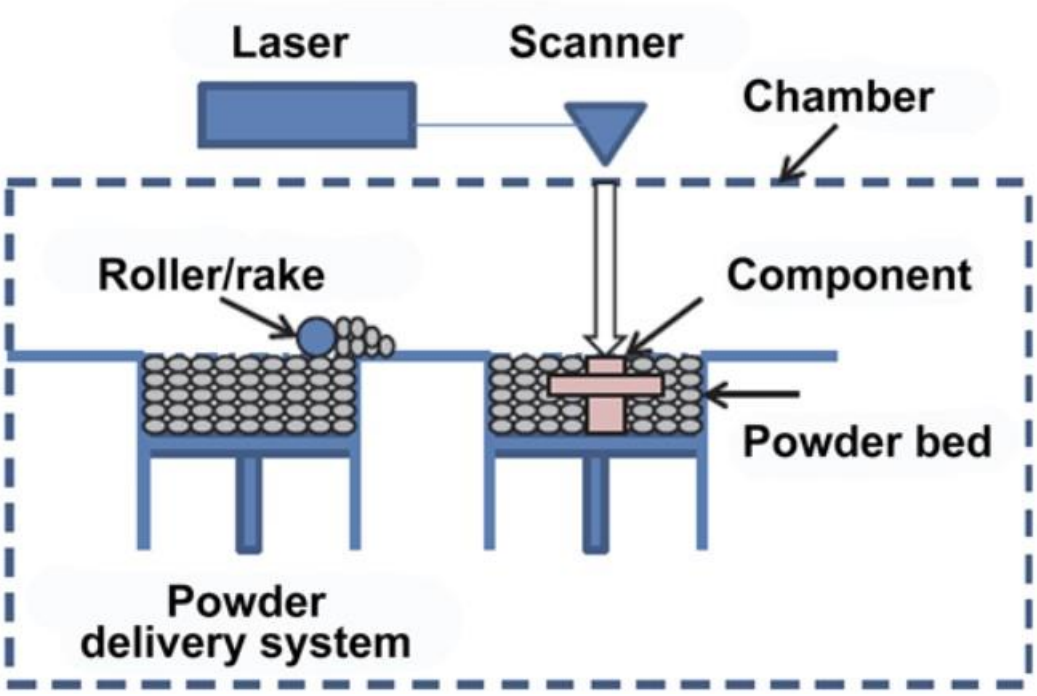

Figure 6: A basic schematic of the PBF process [39].

1.4.2 Direct Energy Deposition

DED functions similarly to PBF in that a metal is melted using a laser or electron beam onto a print bed to form a component layer-by-layer [38]. However, in DED, the metal is fed directly into the laser beam [38]. DED allows for use in a broader array of applications outside of low-volume manufacturing, like part repair, coating, and rapid prototyping [40]. The quality of the parts produced using this method depends on processing parameters like layer thickness, laser power, and feed rate, among others [40]. Inconel 718 has been used extensively in improving this technology for use in additively manufacturing superalloys because of its relatively low cost and ease of manufacturing [38].

1.4.3 Effect of Additive Manufacturing on Properties of Inconel 718

Although additive manufacturing provides many advantages for manufacturing Inconel 718 components, the components' quality is often inferior compared to those produced through casting or forging. The printing parameters must be optimized to reduce the number of pores and cracks upon printing [40]. Even when the printing parameters are optimized, reductions in

performance necessarily occur from processing Inconel 718 in this way. Heating the metal to the temperatures required for additive manufacturing affects the properties of the metal by changing the configuration of precipitates and strengthening elements [38]. Residual stresses arise from uneven cooling rates that can induce distortion and cracking in the material [38]. Furthermore, thermal gradients between layers of the component lead to long, needle-like grains that decrease the material's ductility [33]. Cast Inconel 718 has a yield strength of 915 MPa, an ultimate tensile strength of 1090 MPa, and a ductility of 11% at room temperature [19]. Wrought Inconel 718 has a yield strength of 1185 MPa, an ultimate tensile strength of 1435 MPa, and a ductility of 21% [23]. The data on additively manufactured Inconel 718 has a significant variance, but evidence suggests that the mechanical properties of wrought and cast Inconel 718 can be achieved through additive manufacturing. A study by Smith et al. used direct metal laser sintering with the AMS 5663 heat treatment to achieve a yield strength of 1215 MPa [37]. Zhao, Chen, Lin, and Wong produced Inconel 718 samples using PBF with a yield strength of 1133 MPa, an ultimate tensile strength of 1240 MPa, and ductility of 9% [33]. They applied a unique heat treatment after the samples were printed that increased the properties of the as-printed samples by upwards of 45% [33]. Heat treatment is critical for additively manufactured parts to ensure that the desired mechanical properties are achieved.

1.5 Heat Treatments for Additively Manufactured Inconel 718

Heat treatments specific to additively manufactured Inconel 718 are sparse in scientific literature. However, many of the developed heat treatments are for PBF rather than DED, and this gap in the literature provides an intriguing opportunity for researchers to explore. Table V details several heat treatments found in the literature and the mechanical properties achieved from those heat treatments. The measured mechanical properties from those studies are promising, but there is room for more development. Additionally, the number of samples used in those studies never exceeded nine, so a more comprehensive study with more samples would improve the validity of those studies.

Table V: Selected Heat Treatments for Additively Manufactured Inconel 718 and its Measured Mechanical Properties

Author(s)	Printing Technique Used	Heat Treatment	Mechanical Properties		
			Yield Strength (MPa)	Ultimate Tensile Strength (MPa)	Elongation (%)
Zhao et al. [33]	PBF	1080°C for 1.5 hours; air cool to 980°C and hold for 1 hour; air cool to 720°C and hold for 8 hours; furnace cool to 620°C and hold for 8 hours; air cool	1133	1240	9
Amato et al. [36]	SLM	982°C for .5 hours in vacuum; HIP at 1163°C and .1 GPa for 4 hours in argon	850-930	1140-1200	27-30
Seow et al. [41]	DED	1186°C for 40 minutes; air cool to 980°C and hold for 1 hour; air cool	856	1044	19.9
Kouraytem et al. (a)[42]	PBF	1250°C for 1 hour; furnace cool back to room temperature	830-950	1800-1900	16-20

(a) This study tested components in compression rather than tension. All other reported values are in tension.

In the present study, samples provided by Hermeus will be heat treated using AMS 5663 standard on heat treating Inconel 718. The temperatures for these heat treatments can exceed 1000°C, so caution will be used when treating the samples. The samples will then be tensile tested, and their microstructures will be analyzed to fully understand the effects of the heat treatment on the alloy. The project aims to increase the yield strength, ultimate tensile strength, and ductility of additively manufactured Inconel 718 printed using DED using post-processing standard heat treatments (i.e., AMS 5663/5664) and novel heat treatments comparable to that of cast Inconel 718.

2 Experimental Methods

To begin the study, Inconel samples had to be printed using DED. This was accomplished using a Meltio® printer that Hermeus owned to build a wall of Inconel 718. After the wall had been printed, it was subjected to a stress relief heat treatment before being removed from the build plate. Figure 7 shows a schematic of how the Inconel 718 wall was printed with the appropriate axes.

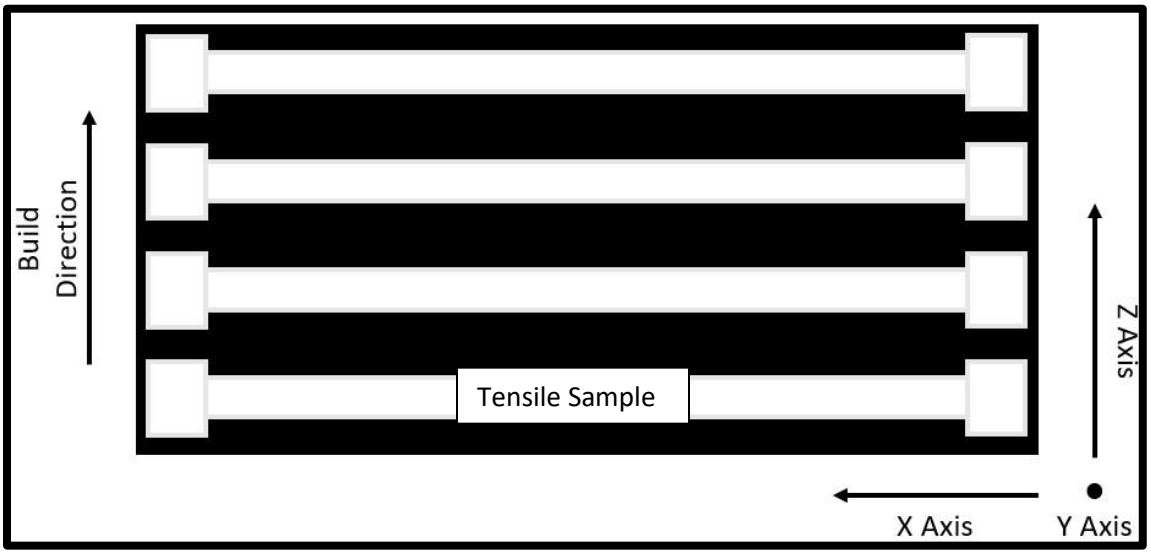

Figure 7: A simplified schematic of how the DED Inconel 718 tensile samples were manufactured prior to being heat treated.

The stress relaxation was a hot isostatic press at 2050°F and 14.5 ksi for 4 hours. Individual tensile samples were then cut from the wall using wire EDM. A total of 12 samples were tested during this study. The gauge length of the samples measured, on average, 32.93 mm in length, 6.40 mm in height, and 6.53 mm in width. The samples were then subjected to a heat treatment in a vacuum so that there was no diffusion of gases into the samples. One sample was not heat treated, so the heat treatment's effects could be analyzed. The heat treatment used on these samples was AMS 5663, which has a schedule as follows: heat to 1750°F and hold for one hour; furnace cool to 1325°F and hold for 8 hours; furnace cool to 1150°F and hold for 8 hours; air cool to room temperature. Once the samples were heat treated, hardness measurements were taken using an HRC indenter. They were then tensile tested using 150 kN Instron to obtain their mechanical properties. The parameters for the tensile test were set using the ASTM E8 standard. The displacement rate of the tensile test was set at 3 mm/min until the samples reached an elongation of 1.5%. The displacement rate then switched to 8 mm/min for the rest of the test. After the samples had been tensile tested, pieces of the sample were cut and mounted in an acrylic matrix for microstructural analysis.

The xz and yz planes of the samples were analyzed so that the layer interfaces of the samples could be analyzed. To prepare the samples for etching, they were first ground on sandpaper lubricated with water. The grit of the sandpaper started at 240 and ended at 600. Then, the samples were polished on fiber pads lubricated with Forgeng's Solution. Final polishing was done on a 0.5-micron polishing pad lubricated with a colloidal silicate solution. Next, the samples were etched by swabbing them with a cotton ball saturated with Modified Kalling's Reagent for 15 seconds. The Modified Kalling's Reagent contained 2 g $CuCl_2$, 40 mL HCl, and 80 mL methanol. Finally, the samples were washed with ethanol and then water before being analyzed under an optical microscope.

3 Results

The data from the mechanical tests are displayed in Table VI. The cast values were obtained from the Metals Handbook and are displayed as goals for the mechanical properties of the heat-treated DED samples.

Table VI: Collected Mechanical Data for Inconel 718

Property	As-printed DED	Heat-treated DED	Heat-treated Cast
Hardness (HRC)	23.1	40	36
Elongation	51.9%	32.33%	12%
Reduction in Area	20.95%	18.98%	15%
Yield Strength (MPa)	546.9	1081	1036
Ultimate Tensile Strength (MPa)	893.7	1199	1240

Figure 8 shows a representative microstructure of the as-printed DED Inconel 718 sample. The xz plane of the sample is being viewed. The layer interfaces show a discoloration caused by the precipitation of the Laves phase. The Laves phase precipitates in Inconel 718 when the material is subjected to high temperatures and rapid cooling rates, which is common at the layer interface of DED components. The grains in this microstructure are large and globular.

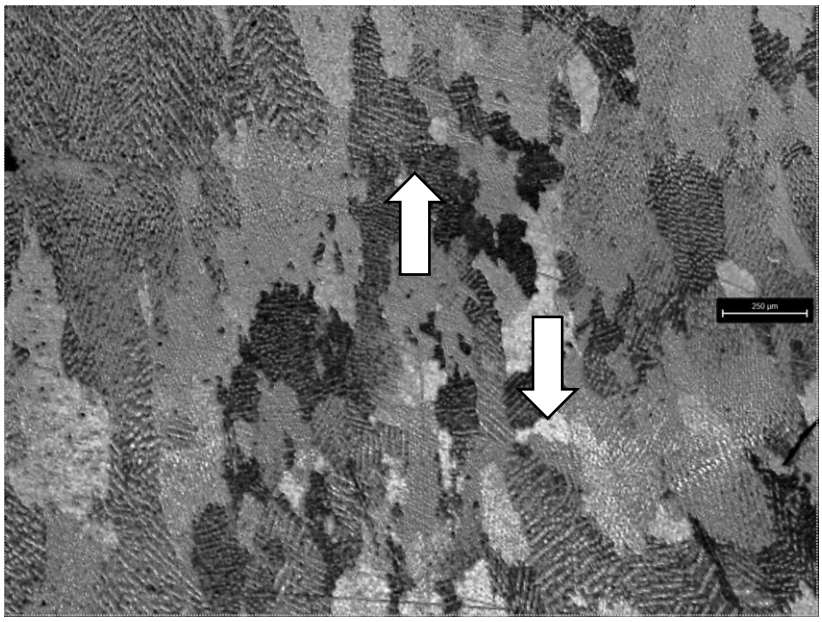

Figure 8: A microstructural image of the xz plane of the as-printed DED Inconel 718. The layer interfaces are denoted by arrows.

The transformation of the DED Inconel 718's microstructure is displayed in Figure 9. Again, the xz plane of the sample is shown. The grains have become more refined, and the layer interfaces have disappeared. The grainy texture of the image is caused by the increased precipitation of the δ phase, which formed small particles throughout the γ matrix, as shown in Figure 10. A more magnified microstructural image is shown in Figure 11 with less δ phase present to illustrate the grain refinement and lack of layer interface.

Figure 9: A microstructural image of the xz plane of a heat-treated DED Inconel 718 sample.

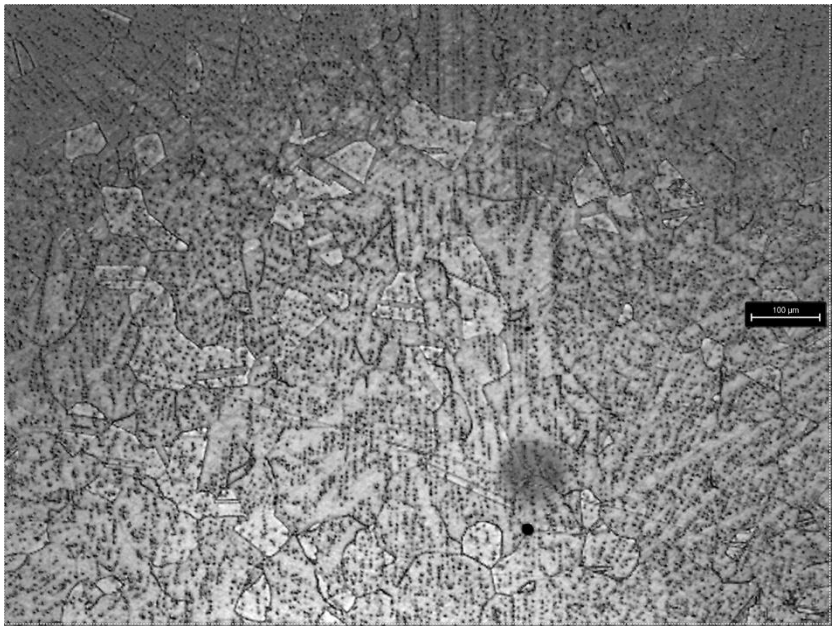

Figure 10: A higher magnification image of Figure 9. The small particles dispersed throughout this image are δ phase precipitates.

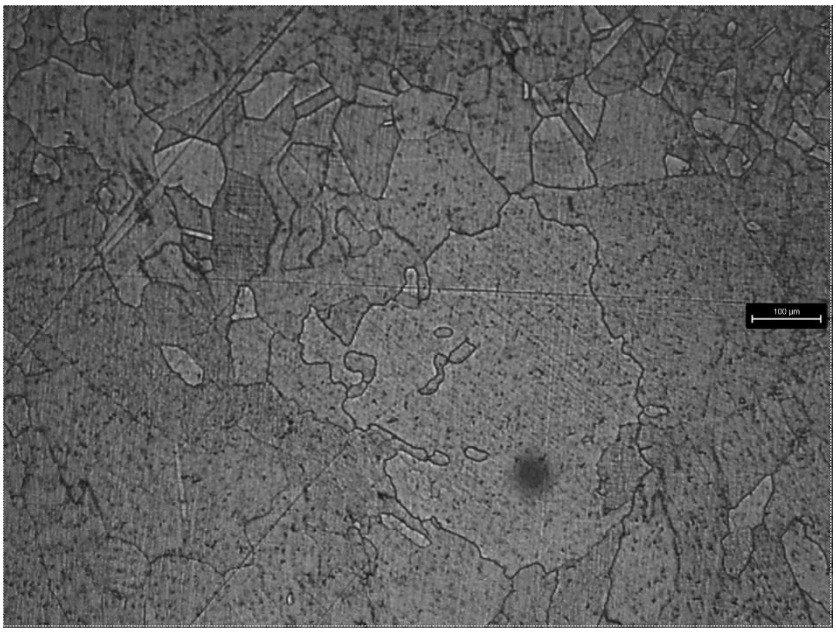

Figure 11: A higher magnification image of Figure 9 with less δ phase present.

The yz plane of the DED Inconel 718 shows a slightly different view of the material. Figure 12 shows a microstructural image of the as-printed DED Inconel 718. The layer interfaces are again pronounced, as well as a columnar grain structure. The columnar grains are caused by epitaxial crystal growth, which is common in additively manufactured metals. The columnar grains are

surrounded by globules of the Laves phase, as shown in Figure 13, which prefers to grow near dendrites of the γ matrix.

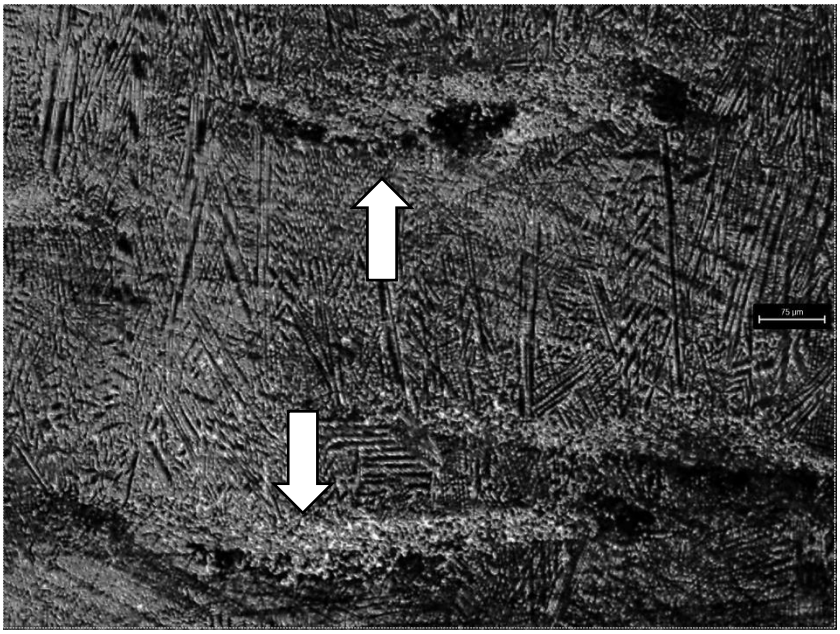

Figure 12: A microstructural image of the yz face of the as-printed DED Inconel 718 sample. The layer interfaces are indicated by arrows.

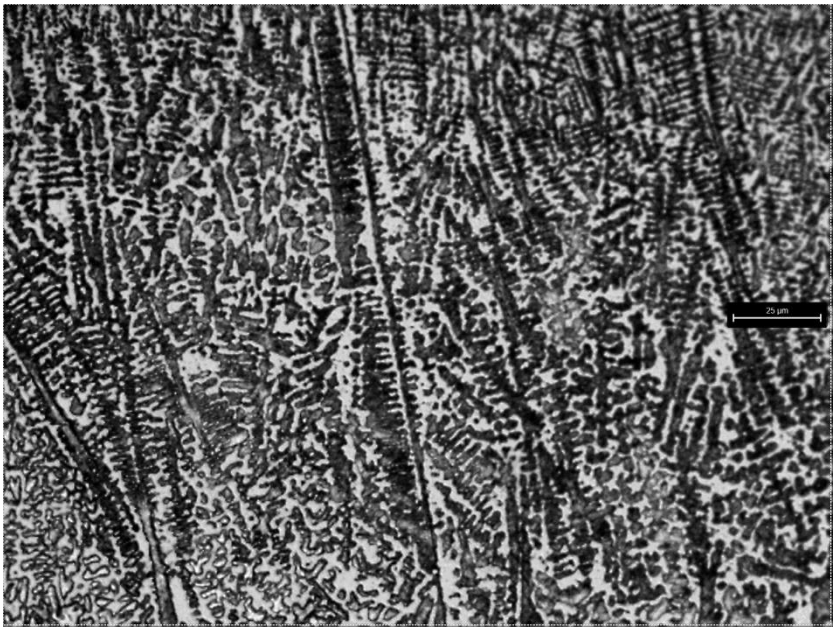

Figure 13: A magnified image of Figure 12. The darker grains are the columnar matrix that are surrounded by globules of the Laves phase.

The yz plane of the heat-treated DED Inconel 718 is similar to that of the xz plane. However, the layer interface is still present in this plane, as seen in Figure 14.

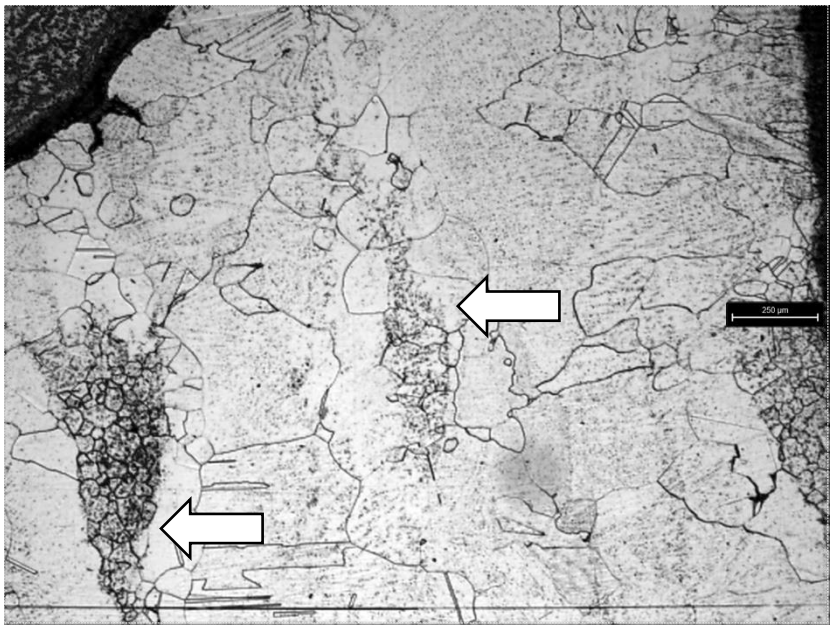

Figure 14: A microstructural image of the yz plane of a heat-treated DED Inconel 718 sample. The layer interfaces are indicated by arrows.

4 Discussion

The heat-treated DED Inconel 718 samples showed significantly improved mechanical properties compared to the as-printed sample. This is expected as Inconel 718 is always heat-treated to some extent to achieve the properties that are require for its applications. More interesting is comparing the heat-treated DED Inconel 718 samples to the heat-treated cast Inconel 718. The DED samples tested achieved similar yield and ultimate tensile strengths to the cast values. Additionally, the DED samples had over twice the elongation of cast Inconel 718. An increase in ductility while yield and ultimate tensile strength stay the same signals an increase in toughness in the DED samples. Greater toughness is valuable in the aerospace industry as it allows mechanical failures in components to be identified and repaired before a catastrophic failure occurs due to fast fracture. Analysis of the microstructures shows that the increase in strength of the DED samples was caused by grain refinement and precipitation of the more beneficial δ phase rather than the Laves phase. While the δ phase is less detrimental to the mechanical

properties of Inconel 718 than the Laves phase, it is still not desirable for best results. The δ phase precipitates when Inconel 718 is overaged, and its prevalence in the previously captured microstructural images shows that the heat treatment was not optimal. It is important to note that no physical defects from the DED process were identified during microstructural analysis.

5 Conclusions

1. The heat treatment used on the DED Inconel 718 samples increased their strength to that of cast Inconel 718.
2. The increase in strength was caused by grain refinement and precipitation of more beneficial phases like the δ phase instead of the Laves phase.
3. The heat treatment used on the DED Inconel 718 samples overaged the material, evidenced by a high amount of δ phase in the γ matrix.

6 Recommendations

1. Test more samples and collect more data to develop a more robust statistical profile.
2. Obtain scanning electron microscope images of the DED Inconel 718's microstructure to observe how the precipitation of the γ' and γ'' phases affected the material's mechanical properties.
3. Alter the heat treatment used to reduce the precipitation of the δ phase. This can be achieved by reducing the time the material is aged in the final step of the AMS 5663 heat treatment.

References

[1] D. Anderson, I. Graham, and B. Williams, *Flight and Motion: The History and Science of Flying*. Taylor & Francis Group, 2011.

[2] K. Bowcutt, "Flying at the Edge of Space and Beyond: The Opportunities and Challenges of Hypersonic Flight," *Bridge (Kans City)*, vol. 50, no. 2, pp. 51–58, Jun. 2020.

[3] M. Summerfield, "The Liquid Propellant Rocket Engine," in *Liquid Propellant Rockets*, Princeton University, 1960, pp. 108–189.

[4] S. Palateerdham, A. Ingenito, and S. Ciprioti, "Experimental Investigation of the Paraffin Thermomechanical Properties and Hybrid Rocket Engine Performance for Different Fuel Grain Formulations," Thesis for Masters in Aerospace Engineering, Sapienza University of Rome, Rome, 2020.

[5] F. Hale, "Hypersonic Aircraft and the National Aerospace Plane," *Encyclopedia of Physical Science and Technology*. North Carolina State University, Raleigh, pp. 365–397, 2003.

[6] K. Bowcutt, "Flying at the Edge of Space and Beyond: The Opportunities and Challenges of Hypersonic Flight," *Bridge (Kans City)*, vol. 50, no. 2, pp. 51–58, Jun. 2020.

[7] V. Babu, "Ramjet Engine," in *Fundamentals of Propulsion*, 1st ed.Springer Cham, 2020, pp. 135–153.

[8] A. Hossain, T. Rahman, and S. Hossain, "Investigation and Improvement of Thermal Efficiency of Hypersonic Scramjet," in *International Mechanical Engineering Congress and Exposition*, Montreal, 2014.

[9] J. Kerrebrock, "Hypersonic Engines," in *Aircraft Engines and Gas Turbines*, 2nd ed.MIT Press, 1992, pp. 401–452.

[10] P. Chaulin, M. Ravel, and A. Gozlan, "Experimental and Design Studies for Turboramjet Combination Engine Volume Vi - Combustion Tests at Les Gatines," Les Gatines, 1966.

[11] A. F. El-Sayed, "Turbine-Based Engines: Turbojet, Turbofan, and Turboramjet Engines," in *Fundamentals of Aircraft and Rocket Propulsion*, London: Springer London, 2016, pp. 403–529. doi: 10.1007/978-1-4471-6796-9_6.

[12] A. Gozlan, "Achievements and Prospects with Composite Air Breathing Engines," *Aircraft Engineering and Aerospace Technology*, vol. 38, no. 2, pp. 10–14, Feb. 1966, doi: 10.1108/eb034120.

[13] E. Heinrich, "Turboramjet engine," GB2241745 (B), Mar. 30, 1994

[14] N. K. Gopinath, K. V. Govindarajan, and R. Mahapatra, "Fluid-thermo-structural response of actively cooled scramjet combustor in hypersonic accelerating-cruise flight," *Int J Heat Mass Transf*, vol. 194, Sep. 2022.

[15] M. Kivy, "Superalloys and Titanium Alloys." California Polytechnic State University, San Luis Obispo, San Luis Obispo, 2022.

[16] M. Aliofkhazraei, Ed., *Superalloys*. InTech, 2015. doi: 10.5772/59358.

[17] R. Reed, "Introduction," in *The Superalloys*, Cambridge University Press, 2006, pp. 1–32. doi: 10.1017/CBO9780511541285.003.

[18] N. S. Stoloff, "Wrought and P/M Superalloys," in *Properties and Selection: Irons, Steels, and High-Performance Alloys*, ASM International, 1990, pp. 950–980. doi: 10.31399/asm.hb.v01.a0001049.

[19] G. L. Erickson, "Polycrystalline Cast Superalloys," in *Properties and Selection: Irons, Steels, and High-Performance Alloys*, ASM International, 1990, pp. 981–994. doi: 10.31399/asm.hb.v01.a0001050.

[20] P. Crook, "Cobalt and Cobalt Alloys," in *Properties and Selection: Nonferrous Alloys and Special-Purpose Materials*, ASM International, 1990, pp. 446–454. doi: 10.31399/asm.hb.v02.9781627081627.

[21] G. L. Erickson, "Polycrystalline Cast Superalloys," in *Properties and Selection: Irons, Steels, and High-Performance Alloys*, ASM International, 1990, pp. 981–994. doi: 10.31399/asm.hb.v01.a0001050.

[22] P. M. Mignanelli *et al.*, “Gamma-gamma prime-gamma double prime dual-superlattice superalloys,” *Scr Mater*, vol. 136, pp. 136–140, Jul. 2017, doi: 10.1016/j.scriptamat.2017.04.029.

[23] N. S. Stoloff, "Wrought and P/M Superalloys," in *Properties and Selection: Irons, Steels, and High-Performance Alloys*, ASM International, 1990, pp. 950–980. doi: 10.31399/asm.hb.v01.a0001049.

[24] T. Philip and T. McCaffrey, "Ultrahigh-Strength Steels," in *Properties and Selection: Irons, Steels, and High-Performance Alloys*, ASM International, 1990, pp. 430–448.

[25] "INCONEL alloy 718," *Special Metals*, Sep. 07, 2007.

[26] W. L. Mankins and S. Lamb, "Nickel and Nickel Alloys," in *Properties and Selection: Nonferrous Alloys and Special Purpose Materials*, ASM International, 1990, pp. 428–445.

[27] R. C. Reed, "The physical metallurgy of nickel and its alloys," in *The Superalloys*, Cambridge University Press, 2006, pp. 33–120. doi: 10.1017/CBO9780511541285.004.

[28] H. Okamoto, M. E. Schlesinger, and E. M. Mueller, Eds., *Alloy Phase Diagrams*. ASM International, 2016. doi: 10.31399/asm.hb.v03.9781627081634.

[29] P. M. Mignanelli *et al.*, “Gamma-gamma prime-gamma double prime dual-superlattice superalloys,” *Scr Mater*, vol. 136, pp. 136–140, Jul. 2017, doi: 10.1016/j.scriptamat.2017.04.029.

[30] I. Dempster and R. Wallis, "Heat Treatment Metallurgy of Nickel-Base Alloys," in *Heat Treating of Nonferrous Alloys*, ASM International, 2016, pp. 399–425. doi: 10.31399/asm.hb.v04e.a0006261.

[31] J. P. Adams, "History of Powder Metallurgy," in *Powder Metallurgy*, ASM International, 2015, pp. 3–8. doi: 10.31399/asm.hb.v07.a0006017.

[32] W. B. James, "Powder Metallurgy Methods and Applications," in *Powder Metallurgy*, ASM International, 2015, pp. 9–19. doi: 10.31399/asm.hb.v07.a0006022.

[33] X. Zhao, J. Chen, X. Lin, and W. Huang, "Study on microstructure and mechanical properties of laser rapid forming Inconel 718," *Materials Science and Engineering: A*, vol. 478, no. 1–2, pp. 119–124, Apr. 2008, doi: 10.1016/j.msea.2007.05.079.

[34] A. Tajyar *et al.*, "Effects of a modified heat-treatment on microstructure and mechanical properties of additively manufactured Inconel 718," *Materials Science and Engineering: A*, vol. 838, Mar. 2022, doi: 10.1016/j.msea.2022.142770.

[35] E. Cakmak *et al.*, "Mechanical Characterization of an Additively Manufactured Inconel 718 Theta-Shaped Specimen," *Metallurgical and Materials Transactions A*, vol. 47, no. 2, pp. 971–980, Feb. 2016, doi: 10.1007/s11661-015-3186-8.

[36] K. N. Amato *et al.*, "Microstructures and mechanical behavior of Inconel 718 fabricated by selective laser melting," *Acta Mater*, vol. 60, no. 5, pp. 2229–2239, Mar. 2012, doi: 10.1016/j.actamat.2011.12.032.

[37] D. H. Smith *et al.*, "Microstructure and mechanical behavior of direct metal laser sintered Inconel alloy 718," *Mater Charact*, vol. 113, pp. 1–9, Mar. 2016, doi: 10.1016/j.matchar.2016.01.003.

[38] B. J. McTiernan, "Powder Metallurgy Superalloys," in *Powder Metallurgy*, ASM International, 2015, pp. 682–702. doi: 10.31399/asm.hb.v07.a0006094.

[39] W. B. James, "Powder Metallurgy Methods and Applications," in *Powder Metallurgy*, ASM International, 2015, pp. 9–19. doi: 10.31399/asm.hb.v07.a0006022.

[40] D.-S. Shim, G.-Y. Baek, J.-S. Seo, G.-Y. Shin, K.-P. Kim, and K.-Y. Lee, "Effect of layer thickness setting on deposition characteristics in direct energy deposition (DED) process," *Opt Laser Technol*, vol. 86, pp. 69–78, Dec. 2016, doi: 10.1016/j.optlastec.2016.07.001.

[41] C. E. Seow, H. E. Coules, G. Wu, R. H. U. Khan, X. Xu, and S. Williams, "Wire + Arc Additively Manufactured Inconel 718: Effect of post-deposition heat treatments on microstructure and tensile properties," *Mater Des*, vol. 183, no. 108157, Dec. 2019, doi: 10.1016/j.matdes.2019.108157.

[42] N. Kouraytem *et al.*, "A recrystallization heat-treatment to reduce deformation anisotropy of additively manufactured Inconel 718," *Mater Des*, vol. 198, no. 109228, Jan. 2021, doi: 10.1016/j.matdes.2020.109228.